J|A|C|S
COMMUNICATIONS

Published on Web 05/27/2007

Long-Range Structural Restraints in Spin-Labeled Proteins Probed by Solid-State Nuclear Magnetic Resonance Spectroscopy

Philippe S. Nadaud, Jonathan J. Helmus, Nicole Höfer,† and Christopher P. Jaroniec*

Department of Chemistry, The Ohio State University, Columbus, Ohio 43210

Received April 3, 2007; E-mail: jaroniec@chemistry.ohio-state.edu

Magic-angle spinning (MAS) solid-state nuclear magnetic resonance (SSNMR) spectroscopy is rapidly developing as a technique for the atomic-level characterization of structure and dynamics of biomacromolecules not amenable to analysis by X-ray crystallography or solution NMR.[1−5] While nearly complete resonance assignments have been achieved for multiple ^{13}C,^{15}N-enriched proteins up to ∼100 aa,[1,2] enabling the determination of relatively high-resolution 3D protein structures in several cases,[6−8] studies of this type are generally hampered by the availability of a limited number of long range (>5 Å) structural restraints.

Here we investigate the possibility of deriving long range (∼10 to 20 Å) restraints from MAS SSNMR spectra of ^{13}C,^{15}N-enriched proteins containing a covalently attached paramagnetic moiety. In general, the presence of unpaired electrons leads to electron-nucleus distance-dependent NMR chemical shift changes and enhanced longitudinal and transverse relaxation rates,[9,10] and these effects have been successfully exploited in solution-state NMR studies of macromolecular structure.[11,12] On the other hand, the majority of MAS NMR studies of paramagnetic solids to date have been carried out on metal coordination complexes,[13−17] and only very recently have the initial applications to paramagnetic metalloproteins been reported.[18−20] We focus here on proteins containing a bound nitroxide spin label. Nitroxide radicals, characterized by relatively large electronic relaxation time constants (T_{1e}, $T_{2e} \geq \sim 100$ ns) and small *g*-anisotropy,[10,11,21] are expected to significantly enhance the transverse relaxation of the neighboring nuclei in immobilized proteins (with rate constant $R_2 \propto \gamma_I^2/r^6$, where γ_I is the gyromagnetic ratio of the nuclear spin *I* and *r* is the electron-nucleus distance), while generating negligible pseudocontact shifts.[10] A nitroxide side-chain (R1) (or its diamagnetic analogue, R1′, used here as a negative control) can be incorporated into proteins using the site-directed spin-labeling approach developed by Hubbell and co-workers[22] (Figure S1, Supporting Information), where a cysteine residue is introduced at the desired position in the protein using site-directed mutagenesis followed by the specific reaction of the thiol group with a suitable reagent.

A model 56 aa protein, B1 immunoglobulin-binding domain of protein G (GB1), was used in this study. GB1, which contains no native cysteines, has been extensively studied using biophysical and spectroscopic techniques, and detailed information about its structure, dynamics, and folding is available, including 3D solution[23] and crystal[24] structures and the complete ^{13}C and ^{15}N resonance assignments in the solid state.[25] R1 and R1′ side-chains were incorporated at solvent-exposed sites in the α-helix (residue 28) and β4-strand (residue 53) as described in the Supporting Information (for brevity the proteins are named 28R1, 28R1′, 53R1, and 53R1′). Solution and SSNMR chemical shifts, and solution transverse relaxation enhancements reveal that these GB1 analogues retain the wild-type fold (Figures S2−S5). SSNMR measurements were performed on (i) microcrystalline ^{13}C,^{15}N-labeled diamagnetic proteins (28R1′ and 53R1′) and (ii) ^{13}C,^{15}N-28R1 (53R1) diluted in a diamagnetic matrix by cocrystallization with natural abundance 28R1′ (53R1′) in ∼1:3 molar ratio (to minimize intermolecular electron−nuclear dipolar couplings).

2D ^{15}N-$^{13}C^{\alpha}$ spectra of 53R1/53R1′ and 28R1/28R1′ acquired at ∼11 kHz MAS rate are shown in Figure 1A,D. Backbone ^{15}N and ^{13}C assignments for 28R1′ and 53R1′ (Figure S5) were obtained using 2D ^{15}N-($^{13}C^{\alpha}$)-^{13}CX, ^{15}N-($^{13}C'$)-^{13}CX, and ^{13}C-^{13}C experiments, and relatively well-resolved correlations (∼50% of residues) are indicated. Notably, ∼25 to 50% of cross-peaks exhibit significantly reduced intensities in the R1 spectra relative to R1′. In addition, ^{15}N-$^{13}C^{\alpha}$ correlations, which are detected in both spectra, display only minor linebroadening for R1 (∼5 to 30 Hz for ^{13}C and ∼2 to 10 Hz for ^{15}N), and essentially identical resonance frequencies indicating negligible pseudocontact shifts. Given that 53R1′ and 28R1′ adopt the GB1 fold, the reduced cross-peak intensities in R1 spectra are found to be highly correlated with the proximity of the corresponding nuclei to the spin label. For example, T25 and V29 (α-helix) are among the least affected correlations in the 53R1 spectrum, whereas I6 (β1-strand) and T49 (loop between β3 and β4) peaks are effectively suppressed. While the precise conformation of R1 (and hence the spin-label location) in 53R1 is currently unknown, the $^{1}H^{N}$, ^{15}N, and $^{13}C^{\alpha}$ atoms are likely to be within ∼10 Å of the electron for I6 and T49, and ∼20 Å away for T25 and V29 (Figure S7). This spin topology is roughly reversed in 28R1 (T25/V29 and I6/T49 are ∼5 to 10 Å and ∼15 to 20 Å from the radical, respectively), resulting in T25/V29 (I6/T49) correlations being among those most (least) suppressed. The modulation of peak intensities, based on each residue's proximity to the electron spin (Figure S7), persists throughout both 53R1 and 28R1. Figure 1 shows the relative cross-peak intensities (heights) in R1/R1′ spectra as a function of residue location in the primary (B,E) and tertiary (C,F) protein structure. For 53R1, the relaxation effects due to the spin label are largest for residues in the β1-β4 strands and connecting loops, while for 28R1 the most strongly affected residues are found in the α-helix and adjacent loops. Note that these data are in qualitative agreement with the solution-state paramagnetic relaxation enhancements for 28R1 and 53R1 shown in Figure S4.

Dipolar contributions to ^{1}H, ^{13}C, and ^{15}N transverse relaxation rates due to the spin label were estimated using the Solomon−Bloembergen equation,[9,10] assuming an electron correlation time of 100 ns (Figures S8 and S9). These calculations indicate that the reduced cross-peak intensities in R1 spectra result primarily from the decay of transverse ^{1}H and ^{13}C coherences during ^{1}H-^{15}N and ^{15}N-$^{13}C^{\alpha}$ cross-polarization (CP) steps, respectively, and are further supported by measurements of magnetization decay during spin-lock pulses (Figure S10). Under our experimental conditions (0.15 ms ^{1}H-^{15}N CP, 3 ms ^{15}N-$^{13}C^{\alpha}$ CP), cross-peaks arising from nuclei within ∼10 Å of the spin label are expected to be at most ∼20% as intense for R1 relative to R1′, even in the absence of additional

† On leave from the Department of Chemical and Environmental Sciences, University of Limerick, Limerick, Ireland.

10.1021/ja072349t CCC: $37.00

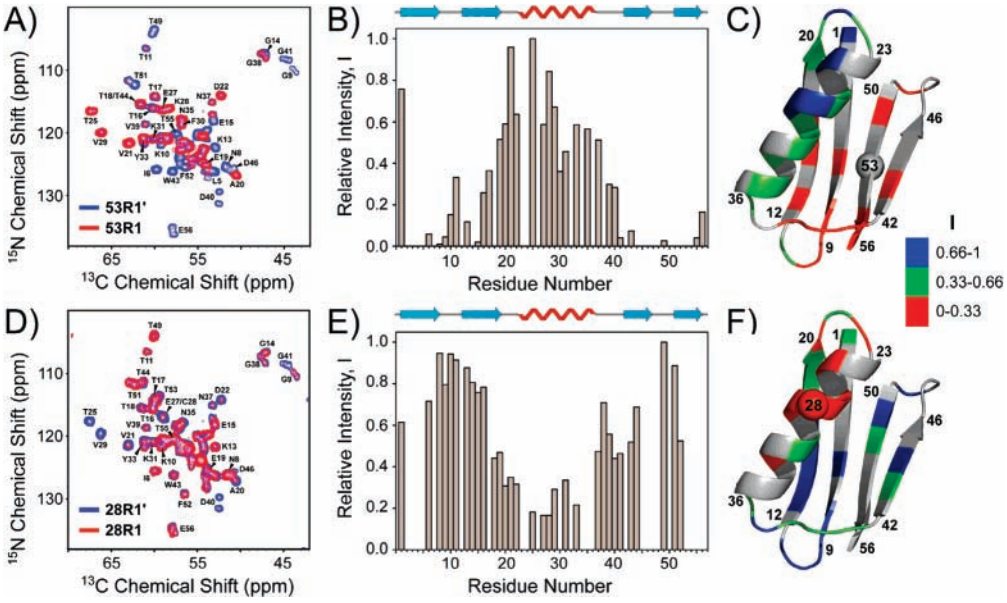

Figure 1. (A) 500 MHz ^{15}N-^{13}C$^{\alpha}$ spectra of 53R1 (red) and 53R1′ (blue) acquired at 11.111 kHz MAS (see Figure S6 for full caption). (B) Relative cross-peak intensities (heights), *I*, in 53R1 and 53R1′ as a function of residue number. To account for possible differences in the amount of ^{13}C,^{15}N-protein in R1 and R1′ samples, we define $I = (I_{R1}/I_{R1'})/(I_{R1}/I_{R1'})_{max}$, where I_{R1} and $I_{R1'}$ are the peak heights in R1 and R1′ spectra and $(I_{R1}/I_{R1'})_{max}$ is the maximum $(I_{R1}/I_{R1'})$ value for the R1/R1′ pair (found here to be ∼0.7 to 0.8). For peaks where no quantitative measurement could be made because of overlap, *I* was set to zero. (C) Ribbon diagram of GB1 (PDB ID: 1pga),[24] with the *I* values mapped onto the structure and color coded as indicated in the figure. Residues for which *I* was not determined are colored in gray, and the R1/R1′ incorporation site is indicated by a sphere on the C$^{\alpha}$ atom. (D−F) Same as panels A−C but for 28R1/28R1′. Typical protein backbone-spin-label distances for secondary structure elements: (28R1) 15−20 Å (β1), 20 Å (β2), 5−10 Å (α), 10−15 Å (β3,β4); (53R1) 10−20 Å (β1), 10−15 Å (β2), 20 Å (α), 10 Å (β3,β4). Estimated uncertainties for individual distances due to unknown R1 conformation are ca. ±2.5 Å (Figure S7).

^{15}N and ^{13}C paramagnetic linebroadening during t_1 and t_2. By contrast, correlations involving nuclei ∼15 to 20 Å away from the radical are expected to retain ∼85 to 95% of the reference intensity and experience only moderate linebroadening in the ^{15}N and ^{13}C dimensions (Figure S8). Although still rather qualitative at this stage, these estimates are consistent with the cross-peak intensities observed experimentally for 28R1/53R1.

In conclusion, we have shown that high-resolution 2D MAS SSNMR spectra recorded on spin-labeled proteins can be used to obtain site-specific structural restraints for nuclei ∼10 to 20 Å from the radical. While the determination of quantitative distance restraints using this approach will, at the very least, require accurate, site-resolved measurements of nuclear relaxation rates (using 3D or 4D pulse schemes incorporating variable relaxation delays), and possibly additional data about electron correlation times and R1 conformation, these restraints provide valuable information about the protein fold on length scales inaccessible to traditional SSNMR methods, even in their current qualitative form. Furthermore, this approach can potentially be extended to editing of SSNMR spectra of larger proteins, with the spin labels used to selectively suppress NMR signals originating from nuclei within ∼10 to 15 Å of the electron and incorporation into proteins of paramagnetic tags with different electronic properties.[26]

Acknowledgment. This research was supported by the Ohio State University. We thank Dr. Angela Gronenborn for the GB1 plasmid, and Drs. Ad Bax, Gareth Eaton, Angela Gronenborn, Junji Iwahara, and Robert Tycko for stimulating discussions.

Supporting Information Available: Experimental part, Figures S1−S10. This material is available free of charge via the Internet at http://pubs.acs.org.

References

(1) McDermott, A. E. *Curr. Opin. Struct. Biol.* **2004**, *14*, 554−561.
(2) Bockmann, A. *C. R. Chim.* **2006**, *9*, 381−392.
(3) Petkova, A. T.; Leapman, R. D.; Guo, Z. H.; Yau, W. M.; Mattson, M. P.; Tycko, R. *Science* **2005**, *307*, 262−265.
(4) Ritter, C.; Maddelein, M. L.; Siemer, A. B.; Luhrs, T.; Ernst, M.; Meier, B. H.; Saupe, S. J.; Riek, R. *Nature* **2005**, *435*, 844−848.
(5) Lange, A.; Giller, K.; Hornig, S.; Martin-Eauclaire, M. F.; Pongs, O.; Becker, S.; Baldus, M. *Nature* **2006**, *440*, 959−962.
(6) Castellani, F.; van Rossum, B.; Diehl, A.; Schubert, M.; Rehbein, K.; Oschkinat, H. *Nature* **2002**, *420*, 98−102.
(7) Zech, S. G.; Wand, A. J.; McDermott, A. E. *J. Am. Chem. Soc.* **2005**, *127*, 8618−8626.
(8) Lange, A.; Becker, S.; Seidel, K.; Giller, K.; Pongs, O.; Baldus, M. *Angew. Chem., Int. Ed.* **2005**, *44*, 2089−2092.
(9) Solomon, I. *Phys. Rev.* **1955**, *99*, 559−565.
(10) Bertini, I.; Luchinat, C. *Coord. Chem. Rev.* **1996**, *150*, 1−292.
(11) Kosen, P. A. *Methods Enzymol.* **1989**, *177*, 86−121.
(12) Bertini, I.; Luchinat, C.; Parigi, G.; Pierattelli, R. *Chembiochem* **2005**, *6*, 1536−49.
(13) Chacko, V. P.; Ganapathy, S.; Bryant, R. G. *J. Am. Chem. Soc.* **1983**, *105*, 5491−5492.
(14) Brough, A. R.; Grey, C. P.; Dobson, C. M. *J. Am. Chem. Soc.* **1993**, *115*, 7318−7327.
(15) Liu, K.; Ryan, D.; Nakanishi, K.; McDermott, A. E. *J. Am. Chem. Soc.* **1995**, *117*, 6897−6906.
(16) Wickramasinghe, N. P.; Ishii, Y. *J. Magn. Reson.* **2006**, *181*, 233−243.
(17) Kervern, G.; Pintacuda, G.; Zhang, Y.; Oldfield, E.; Roukoss, C.; Kuntz, E.; Herdtweck, E.; Basset, J. M.; Cadars, S.; Lesage, A.; Coperet, C.; Emsley, L. *J. Am. Chem. Soc.* **2006**, *128*, 13545−13552.
(18) Jovanovic, T.; McDermott, A. E. *J. Am. Chem. Soc.* **2005**, *127*, 13816−13821.
(19) Pintacuda, G.; Giraud, N.; Pierattelli, R.; Bockmann, A.; Bertini, I.; Emsley, L. *Angew. Chem., Int. Ed.* **2007**, *119*, 1097−1100.
(20) Balayssac, S.; Bertini, I.; Lelli, M.; Luchinat, C.; Maletta, M. *J. Am. Chem. Soc.* **2007**, *129*, 2218−2219.
(21) Eaton, S. S.; Eaton, G. R. In *Distance Measurements in Biological Systems by EPR;* Biological Magnetic Resonance, Vol. 19; Kluwer Academic: New York, 2000.
(22) Hubbell, W. L.; Altenbach, C. *Curr. Opin. Struct. Biol.* **1994**, *4*, 566−573.
(23) Gronenborn, A. M.; Filpula, D. R.; Essig, N. Z.; Achari, A.; Whitlow, M.; Wingfield, P. T.; Clore, G. M. *Science* **1991**, *253*, 657−661.
(24) Gallagher, T.; Alexander, P.; Bryan, P.; Gilliland, G. L. *Biochemistry* **1994**, *33*, 4721−4729.
(25) Franks, W. T.; Zhou, D. H.; Wylie, B. J.; Money, B. G.; Graesser, D. T.; Frericks, H. L.; Sahota, G.; Rienstra, C. M. *J. Am. Chem. Soc.* **2005**, *127*, 12291−12305.
(26) Rodriguez-Castaneda, F.; Haberz, P.; Leonov, A.; Griesinger, C. *Magn. Reson. Chem.* **2006**, *44*, S10−S16.

JA072349T

Supporting Information

Long Range Structural Restraints in Spin Labeled Proteins Probed by Solid-State NMR Spectroscopy

Philippe S. Nadaud, Jonathan J. Helmus, Nicole Höfer,[†] and Christopher P. Jaroniec*

Department of Chemistry, The Ohio State University, Columbus, Ohio 43210
[†]On leave from: *Department of Chemical and Environmental Sciences, University of Limerick, Limerick, Ireland*
E-mail: jaroniec@chemistry.ohio-state.edu

Experimental Section

a. Construction of GB1 Cysteine Mutants. Plasmid DNA corresponding to the T2Q mutant of the B1 immunoglobulin-binding domain of protein G (subsequently referred to as GB1) was kindly provided by Dr. A. M. Gronenborn (University of Pittsburgh). The T2Q mutation reduces the cleavage of the N-terminal Met residue, and has a minimal effect on the protein structure, dynamics and folding.[1] Plasmids encoding for cysteine mutations at positions K28 or T53 of wild-type (wt) GB1, which contains no native cysteine residues, were constructed using the GB1 plasmid DNA, appropriate primers (Invitrogen, Carlsbad, CA) and the QuikChange II site-directed mutagenesis protocol (Stratagene, La Jolla, CA), and confirmed by DNA sequencing of the entire genes (Davis Sequencing, Davis, CA).

These mutations correspond to solvent exposed sites in the α-helix (K28) and the β4-strand (T53) of GB1, and were selected for this study since they were not expected to significantly perturb the structure or oligomeric state of wt GB1 (A. M. Gronenborn, personal communication). This was confirmed to indeed be the case by measuring solution and solid-state NMR chemical shifts and paramagnetic relaxation enhancements in solution (Figures S2-S5). It is important to note here that although the known three-dimensional structure of GB1 was helpful in identifying suitable modification sites in this study it should also be possible to successfully introduce spin labels into proteins of unknown structure using an approach, which combines secondary structure information obtained from NMR chemical shift data for the wt protein with the analysis of hydrophilicity patterns to identify likely solvent-accessible residues,[2] as discussed recently by Battiste and Wagner.[3] Moreover, spin labels can be readily introduced into different secondary structure elements with minimal effects on the protein fold as shown by previous EPR[4] and solution-state NMR[3,5] studies, and their influence on protein structure can be conveniently assessed by comparing NMR chemical shifts for the wt and modified proteins.

b. Protein Expression and Purification. *E. coli* BL21(DE3) cells (Invitrogen), transformed with K28C or T53C GB1 plasmids, were used to inoculate 2 mL of Luria-Bertani (LB) medium containing 100 μg/mL ampicilin and grown at 37 ^{o}C for 8 h. A 25 μL aliquot of the LB culture was used to inoculate 25 mL of fresh LB medium (for expression of unlabeled proteins) or 25 mL of a modified M9 minimal medium,[6] which contained 1 g/L $^{15}NH_4Cl$, 3 g/L ^{13}C-glucose and 0.5 g/L of ^{13}C,^{15}N-labeled rich-medium supplement (Isogro, Isotec, Inc.) (for expression of ^{13}C,^{15}N-labeled proteins) and grown overnight. The 25 mL LB and M9 overnight cultures were transferred into 1 L of fresh LB medium (for unlabeled proteins) or 1 L of fresh ^{13}C,^{15}N-enriched M9 medium (for ^{13}C,^{15}N-labeled proteins),

respectively, and grown until the culture reached an OD_{600} of ~0.8. Protein expression was induced by addition of isopropyl β-D-thiogalactoside to a final concentration of 0.5 mM and cell growth was continued for 4 h.

Cells were harvested by centrifugation at 4,000 × g for 10 min at 4 ^{o}C, resuspended in 40 mL of phosphate buffered saline (1.7 mM KH_2PO_4, 5mM Na_2HPO_4, 150 mM NaCl, pH 7.4) containing 5 mM dithiothreitol (DTT), heated at 80 ^{o}C for 5 min, chilled on ice for 15 min, followed by centrifugation at 30,000 × g for 30 min at 4 ^{o}C. The supernatant was concentrated using Amicon Ultra-15 5,000 MWCO devices (Millipore, Billerica, MA), and the proteins were purified at room temperature by gel filtration chromatography using a HiPrep 26/60 Sephacryl S-100 or HiLoad 16/60 Superdex 75 prep grade column (Amersham Biosciences/GE Healthcare) equilibrated with a 50 mM sodium phosphate, 150 mM NaCl, 5 mM DTT, pH 6.5 buffer. Peak fractions containing the proteins were concentrated using Amicon Ultra-15 5,000 MWCO devices. Typical yields (determined from absorbance at 280 nm with $\varepsilon = 9970\ M^{-1}\cdot cm^{-1}$) were 40-50 mg per 1 L of culture for ^{13}C,^{15}N-labeled proteins, and 60-80 mg per 1 L culture for unlabeled proteins, and the proteins were characterized using electrospray ionization mass spectrometry and solution-state NMR. A wild-type GB1 reference sample was also prepared using the same procedure, but without the use of DTT during cell lysis and protein purification.

c. Spin Labeling of Proteins. A nitroxide spin label side-chain (designated as R1; Figure S1) was introduced[7] into ^{13}C,^{15}N-labeled K28C and T53C GB1 as follows (for brevity the R1-modified proteins are referred to as 28R1 and 53R1, respectively). DTT was removed from the buffer using a HiPrep 26/10 desalting column or a series of five HiTrap 5 ml desalting columns (Amersham Biosciences/GE Healthcare) equilibrated with 50 mM sodium phosphate, pH 6.5. Immediately thereafter, the proteins were incubated overnight at 4 ^{o}C with a 5-fold molar excess of the nitroxide spin label reagent, (1-oxyl-2,2,5,5-tetramethyl-Δ3-pyrroline-3-methyl)-methanethiosulfonate,[8] purchased from Toronto Research Chemicals Inc. (Toronto, ON, Canada). The unreacted methanethiosulfonate reagent was removed using a desalting column and the proteins were concentrated using Amicon Ultra-15 5,000 MWCO devices.

d. Preparation of Diamagnetic Analogue Proteins. For the initial characterization of the R1-induced paramagnetic relaxation enhancements (PRE) of amide ^{1}H and ^{15}N nuclei in solution (Figure S4), the diamagnetic analogues of 28R1 and 53R1, required for the acquisition of reference ^{1}H-^{15}N heteronuclear single-quantum correlation (HSQC) NMR spectra, were prepared directly inside the NMR sample tube by reducing the nitroxide spin label to a hydroxylamine using a 5-fold molar excess of sodium ascorbate.[9] Since the reduction of nitroxides by ascorbate is known to be a reversible process[10] (we

confirmed that this was indeed the case under the experimental conditions employed in this work), for the solid-state NMR studies we prepared GB1 mutants (both natural abundance (NA) and $^{13}C,^{15}N$-labeled) containing a 'permanent' diamagnetic analogue of R1,[11] designated as R1′ (Figure S1). This was done by reacting K28C and T53C GB1 with (1-acetyl-2,2,5,5-tetramethyl-Δ3-pyrroline-3-methyl)methanethiosulfonate (Toronto Research Chemicals) as described above for the spin labeled methanethiosulfonate reagent. As expected based on the very minor structural differences between the R1 and R1′ side-chains,[11] the 2D ^{1}H-^{15}N HSQC NMR spectra of 28R1′ and 53R1′ were essentially superimposable with the ascorbate-reduced spectra of 28R1 and 53R1, respectively (data not shown); quantitative analysis of HSQC spectra for 53R1′ and reduced 53R1 revealed negligible average absolute chemical shift differences (0.008 ± 0.008 ppm for $^{1}H^{N}$ and 0.08 ± 0.12 ppm for ^{15}N).

e. Solution-State NMR Spectroscopy. Samples for solution-state backbone $^{1}H^{N}$, ^{15}N and ^{13}C resonance assignments of reduced 28R1 and 53R1 were prepared by dissolving $^{13}C,^{15}N$-labeled proteins at a concentration of ~1 mM in an H_2O solution containing 50 mM sodium phosphate, 5 mM sodium ascorbate, 7% D_2O, and 0.02% (w/v) NaN_3 at pH 6.5 in a total volume of 500 μL. A reference ~1 mM $^{13}C,^{15}N$-GB1 sample was prepared using the same buffer, but containing no ascorbate. For the NMR measurements the samples were transferred to 5 mm sample tubes (Wilmad-Labglass, Buena, NJ). Experiments were performed at 25 ^{o}C using a 600 MHz Bruker spectrometer equipped with a triple resonance pulsed field gradient probe, optimized for ^{1}H detection. $^{1}H^{N}$, ^{15}N, $^{13}C'$, $^{13}C^{\alpha}$ and $^{13}C^{\beta}$ resonance assignments for GB1, and ascorbate-reduced 28R1 and 53R1 were obtained using 3D HNCO, HNCA, and HN(CA)CB experiments based on pulse schemes of Yamazaki et al.[12] Data were processed using NMRPipe[13] and analyzed using Sparky.[14] Chemical shifts were referenced relative to TSP, and the resonance assignments of GB1 and reduced 28R1/53R1 are compared in Figure S3.

f. Solid-State NMR Samples. Two types of $^{13}C,^{15}N$-enriched microcrystalline protein samples were used for the solid-state NMR measurements: (i) diamagnetic controls needed to record the reference spectra and (ii) spin-labeled proteins. For the diamagnetic samples, solutions containing $^{13}C,^{15}N$-28R1′ and $^{13}C,^{15}N$-53R1′ were concentrated to ~30 mg/mL in 50 mM sodium phosphate pH 6.5 buffer containing 0.02% (w/v) NaN_3 using Amicon Ultra-4 5,000 MWCO devices. Protein microcrystals were prepared by microdialysis at 4 ^{o}C, using microdialysis buttons purchased from Hampton Research (Aliso Viejo, CA), with a precipitant solution containing 2-methylpentane-2,4-diol, isopropanol, and deionized water in a 2:1:1 (v/v) ratio, and the crystallization was allowed to proceed for at least 48 h. The spin-labeled protein microcrystals were prepared exactly as described above, but rather than using

pure ^{13}C,^{15}N-28R1 and ^{13}C,^{15}N-53R1, the ^{13}C,^{15}N-enriched spin labeled proteins were co-crystallized with their corresponding natural abundance, diamagnetic counterparts (NA-28R1′ and NA-53R1′) in ~1:3 molar ratio. This results in the protein ^{13}C and ^{15}N nuclei being primarily influenced by the covalently-attached nitroxide spin label (and not by other spin labels in the crystal lattice), while concurrently retaining reasonable sensitivity of the ^{13}C and ^{15}N NMR spectra. The resulting protein microcrystals were center-packed in 3.2 mm Varian rotors by centrifugation. The amounts of ^{13}C,^{15}N labeled 28R1, 28R1′, 53R1 and 53R1′ in the final NMR samples were estimated as ~3 ± 1 mg, by comparing the overall spectral intensities observed in 1D ^{13}C Bloch decay and ^{15}N cross-polarization spectra to the corresponding intensities in previously characterized control samples of wt GB1.

g. Solid-state NMR Spectroscopy. Experiments were performed on a three-channel Varian spectrometer operating at the frequencies of 499.8 MHz for ^{1}H, 125.7 for ^{13}C and 50.6 MHz for ^{15}N, and equipped with a 3.2 mm Varian BioMAS probe.[15] The MAS frequency was 11.111 kHz, regulated to ca. ± 3 Hz, and the sample temperature was controlled by using a stream of compressed air, delivered to the sample at a flow rate of ca. 30 L/min. The compressed air temperature was set to 273 K, resulting in an effective sample temperature of ca. 278 K as determined by lead nitrate calibration.[16] Typical ^{1}H, ^{13}C and ^{15}N 90^{o} pulse lengths employed in the experiments were 2.5 μs, 5.0 μs and 6.0 μs, respectively, and during indirect chemical shift evolution periods and FID acquisition, TPPM proton decoupling[17] was applied at a field strength of ~70 kHz (pulse length 7.0 μs, total phase difference 7.0^{o}). Parameters used to acquire the 2D ^{15}N-$^{13}C^{\alpha}$ correlation spectra for 53R1, 53R1′, 28R1 and 28R1′ (Figures 1 and S6) were as follows: ^{15}N carrier at ~120 ppm, ^{13}C carrier at ~80 ppm, ^{1}H-^{15}N CP (^{1}H field ~50 kHz, ^{15}N field ~40 kHz, contact time 150 μs), ^{15}N-$^{13}C^{\alpha}$ SPECIFIC CP[18] (^{15}N field ~28 kHz, ^{13}C field ~17 kHz with a tangent ramp of ± 0.5 kHz,[19] ^{1}H field 100 kHz CW, contact time 3 ms).

Nearly complete ^{15}N and $^{13}C^{\alpha}$ resonance assignments for 53R1′ and 28R1′ were obtained using a set of three 2D correlation experiments: ^{13}C-^{13}C, ^{15}N-($^{13}C^{\alpha}$)-^{13}CX, and ^{15}N-($^{13}C'$)-^{13}CX.[20] The acquisition parameters were as follows, 2D ^{13}C-^{13}C: ^{13}C carrier at ~100 ppm, ^{1}H-^{13}C CP (^{1}H field ~50 kHz, ^{13}C field ~40 kHz with a linear ramp of ± 2 kHz,[21] contact time 1 ms), ^{13}C-^{13}C correlations established using proton driven spin-diffusion (PDSD) mixing of 5 ms duration, enhanced by the application of a rotary resonant ^{1}H field (n=1, 11.1 kHz);[22-24] 2D ^{15}N-($^{13}C^{\alpha}$)-^{13}CX: ^{15}N carrier at ~120 ppm, ^{13}C carrier at ~80 ppm, ^{1}H-^{15}N CP (^{1}H field ~50 kHz, ^{15}N field ~40 kHz with a linear ramp of ± 2 kHz, contact time 1 ms), ^{15}N-$^{13}C^{\alpha}$ SPECIFIC CP (^{15}N field ~28 kHz, ^{13}C field ~17 kHz with a tangent ramp of ± 0.5 kHz, ^{1}H field 100 kHz CW, contact time 3 ms), 15 ms PDSD (with n=1 rotary resonant field) ^{13}C-^{13}C mixing; 2D ^{15}N-($^{13}C'$)-^{13}CX: ^{15}N carrier at ~120 ppm, ^{13}C carrier at ~175 ppm, ^{1}H-^{15}N CP

(^{1}H field ~50 kHz, ^{15}N field ~40 kHz with a linear ramp of ± 2 kHz, contact time 1 ms), ^{15}N-$^{13}C^{\alpha}$ SPECIFIC CP (^{15}N field ~39 kHz, ^{13}C field ~27 kHz with a tangent ramp of ± 1 kHz, ^{1}H field 100 kHz CW, contact time 6 ms), 15 ms PDSD (with n=1 rotary resonant field) ^{13}C-^{13}C mixing. Data were processed using NMRPipe,[13] analyzed using Sparky,[14] and chemical shifts were referenced relative to DSS as described by Marcombe and Zilm.[25] Selected assignments, corresponding to well-resolved correlations, are indicated in Figures 1 and S6, and a quantitative comparison of $^{13}C^{\alpha}$, $^{13}C^{\beta}$ and ^{15}N solid-state NMR chemical shifts for 28R1′, 53R1′ and wt GB1 is shown in Figure S5.

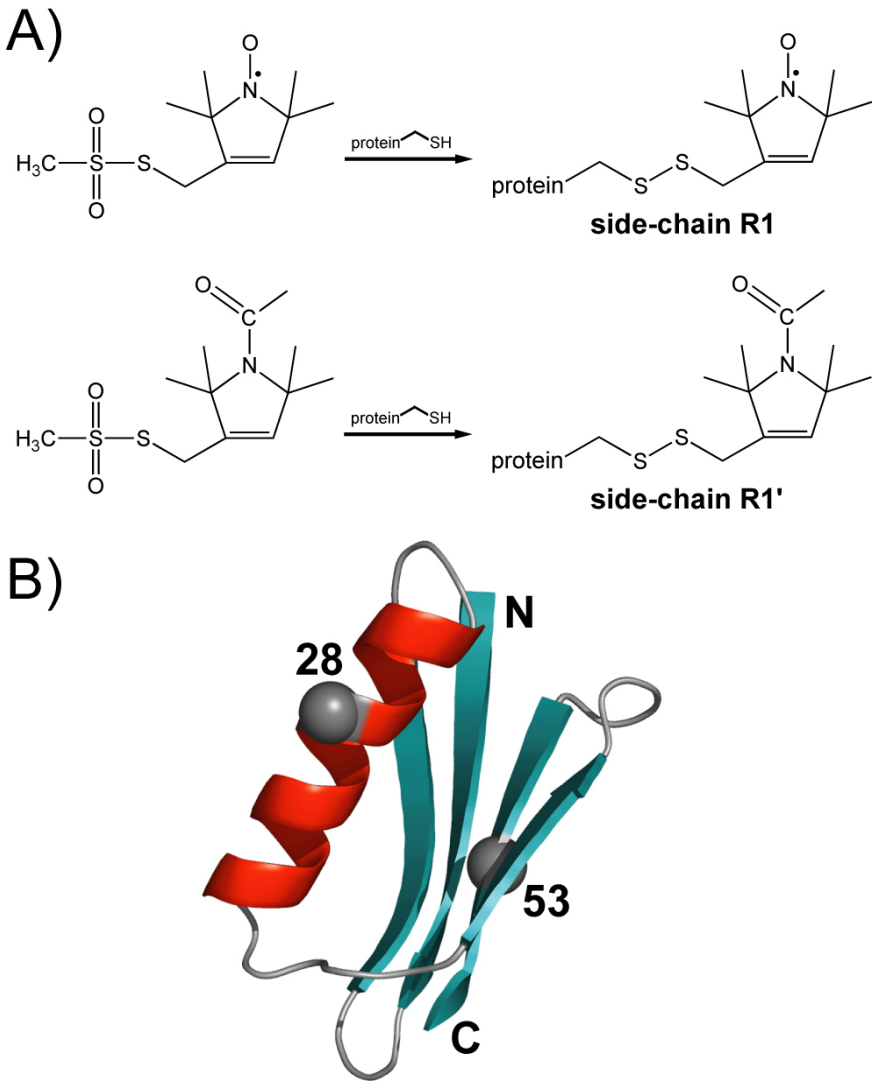

Figure S1. (A) Modification of cysteine residues in proteins[7] using a nitroxide spin-label reagent[8] and its diamagnetic analogue,[11] yielding side-chains R1 and R1', respectively. (B) Ribbon diagram of GB1 (PDB ID: 1pga),[26] with R1/R1′ incorporation sites indicated by gray spheres on the C^{α} atoms. The resulting proteins are designated as 28R1, 28R1′, 53R1, and 53R1′.

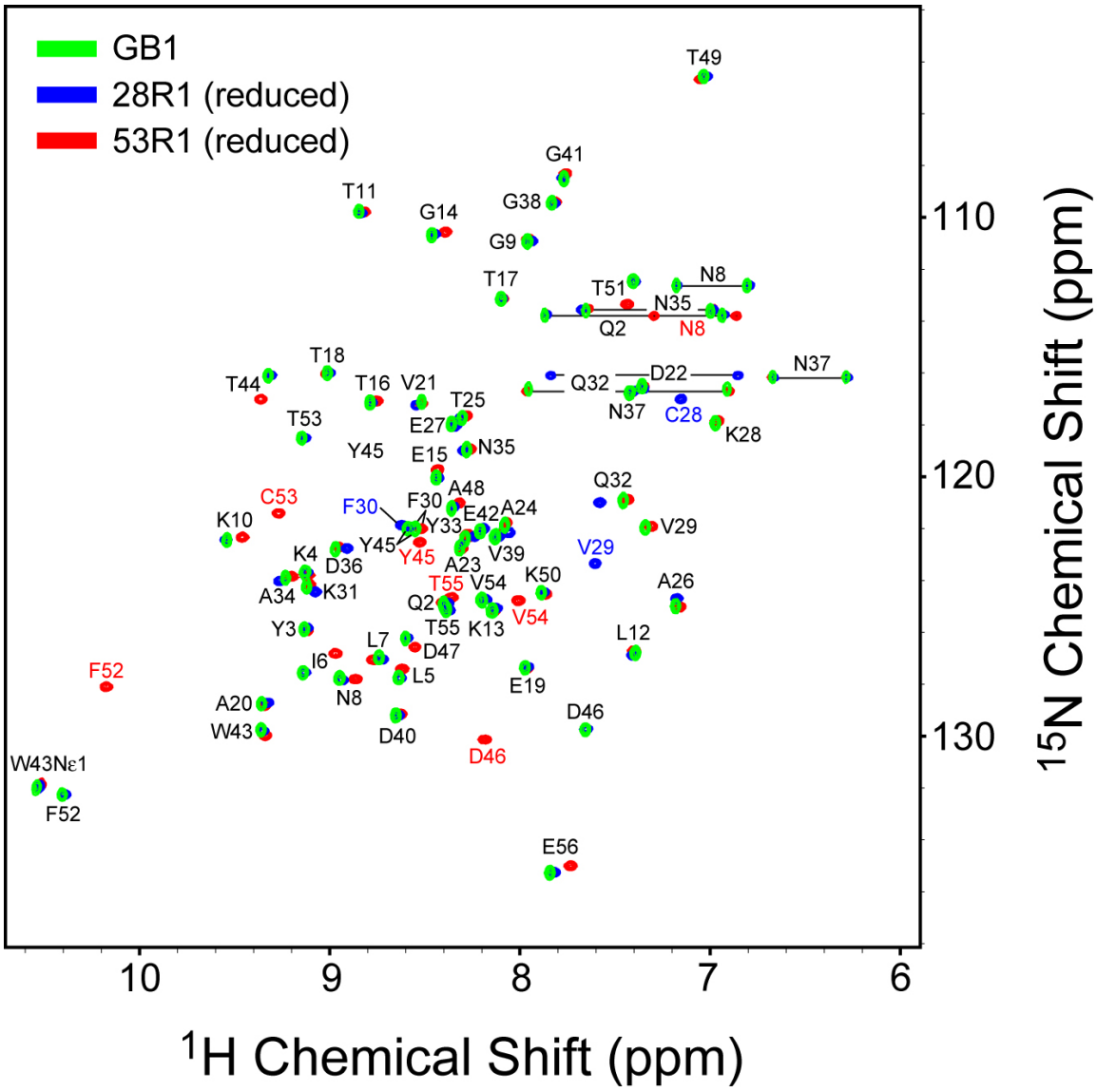

Figure S2. 600 MHz ^{1}H-^{15}N HSQC NMR spectra of wt GB1 (green contours), and ascorbate-reduced 28R1 (blue contours) and 53R1 (red contours). $^{1}H^{N}$ and ^{15}N resonance assignments were obtained at 25 ^{o}C using ~1 mM protein samples and 3D HNCA and HN(CA)CB experiments as described above, and Asn and Gln side-chain NH_2 assignments are based on published data.[27] Resonances displaying minimal chemical shift differences between wt GB1 and 28R1 and/or 53R1 are labeled in black font, while resonances displaying more substantial chemical shift differences for 28R1 or 53R1 relative to wt GB1 are labeled in blue and red fonts, respectively. Overall, few $^{1}H^{N}$ and ^{15}N chemical shift differences greater than 0.1 and 0.5 ppm, respectively, are observed for ascorbate-reduced 28R1 and 53R1 relative to wt GB1 (see Figure S3 for a quantitative analysis of $^{1}H^{N}$, ^{15}N, $^{13}C'$, $^{13}C^{\alpha}$ and $^{13}C^{\beta}$ chemical shift differences), which indicates that K28C and T53C mutations followed by R1 side-chain modification do not significantly perturb the three-dimensional structure or the oligomeric state of wt GB1 in solution. These results are consistent with previous EPR[4] and solution-state NMR[3,5] studies which found that in most cases properly placed nitroxide spin label side-chains have a minimal effect on the protein fold.

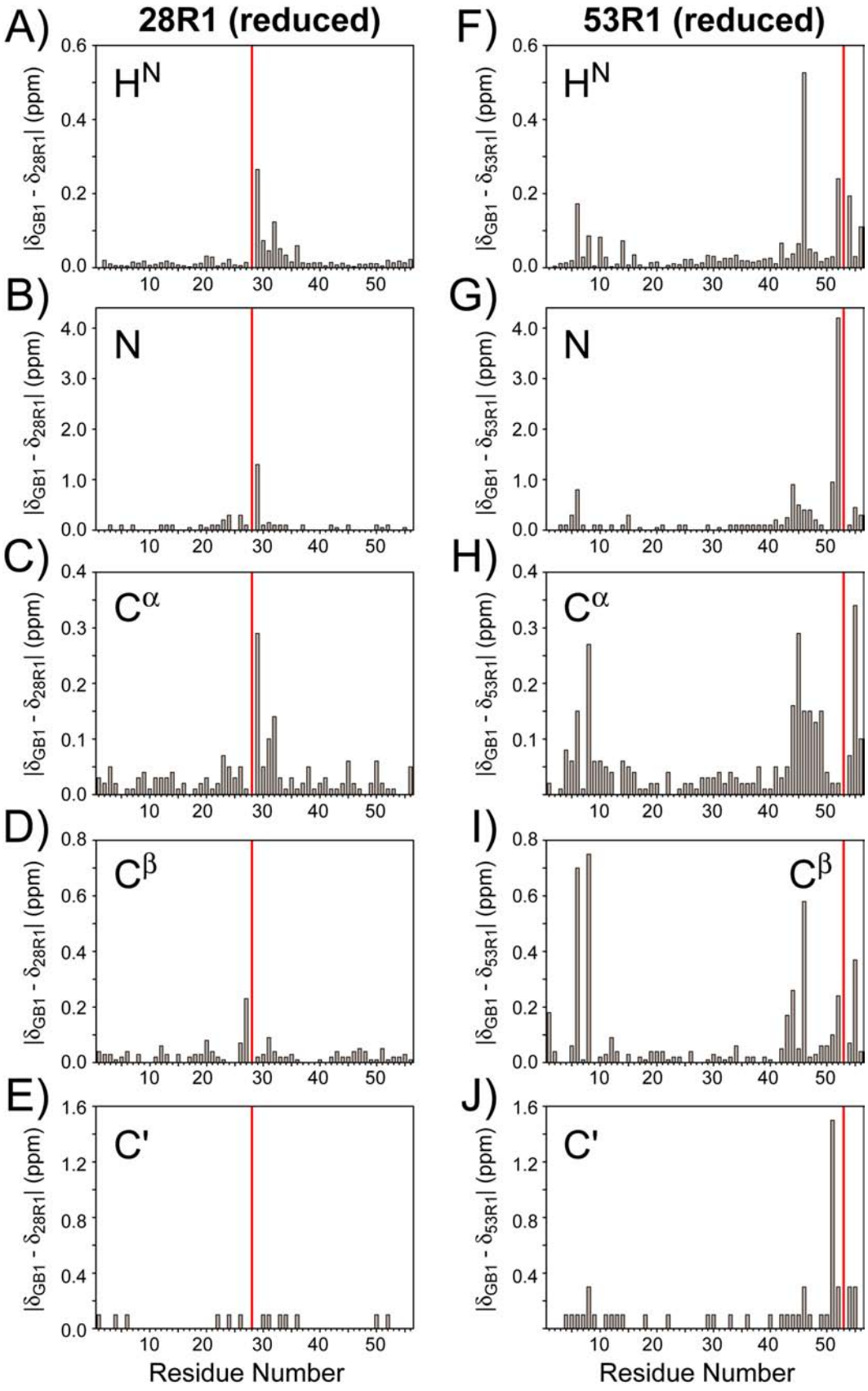

Figure S3. Quantitative analysis of solution-state chemical shift differences for ascorbate-reduced 28R1 (A-E) and 53R1 (F-J) relative to wt GB1. Absolute chemical shift differences in ppm as a function of residue number are shown for $^{1}H^{N}$, ^{15}N, $^{13}C'$, $^{13}C^{\alpha}$ and $^{13}C^{\beta}$ nuclei (nucleus type indicated directly in the plot), and the mutation

sites (residue 28 in A-E and residue 53 in F-J) are indicated by vertical red lines. The average absolute chemical shift differences, $\langle|\Delta\delta|\rangle$, of 28R1 relative to wt GB1 were: $\langle|\Delta\delta(H^N)|\rangle$ = 0.02 ± 0.04 ppm, $\langle|\Delta\delta(N)|\rangle$ = 0.08 ± 0.18 ppm, $\langle|\Delta\delta(C^\alpha)|\rangle$ = 0.03 ± 0.04 ppm, $\langle|\Delta\delta(C^\beta)|\rangle$ = 0.03 ± 0.03 ppm, and $\langle|\Delta\delta(C')|\rangle$ = 0.02 ± 0.04 ppm. For 53R1 the differences were: $\langle|\Delta\delta(H^N)|\rangle$ = 0.05 ± 0.08 ppm, $\langle|\Delta\delta(N)|\rangle$ = 0.2 ± 0.6 ppm, $\langle|\Delta\delta(C^\alpha)|\rangle$ = 0.06 ± 0.07 ppm, $\langle|\Delta\delta(C^\beta)|\rangle$ = 0.09 ± 0.17 ppm, and $\langle|\Delta\delta(C')|\rangle$ = 0.10 ± 0.21 ppm. Note that the $^{13}C'$ chemical shift for E56 was not measured, and the following shifts were not applicable: $^1H^N$ and ^{15}N for M1, and $^{13}C^\beta$ for G9, G14, G38 and G41. The shift differences involving these atoms, as well as all shift differences involving the mutated residues (residues 28 and 53 for 28R1 and 53R1, respectively) were set to zero in the plots and excluded from the calculated averages. For 28R1 the main chemical shift differences are found to be in the immediate vicinity of the mutation site (residues 26-32) as expected.[3,5] For 53R1, in addition to the mutation site (residues 51-56), moderate chemical shift differences are also observed for residues 6 and 8 (found in the β1-strand) and 44-46 (β3-strand) in the spatial vicinity of the modification site, and most likely reflect the interactions between the R1 side-chain and the side-chains of the aforementioned residues.[3]

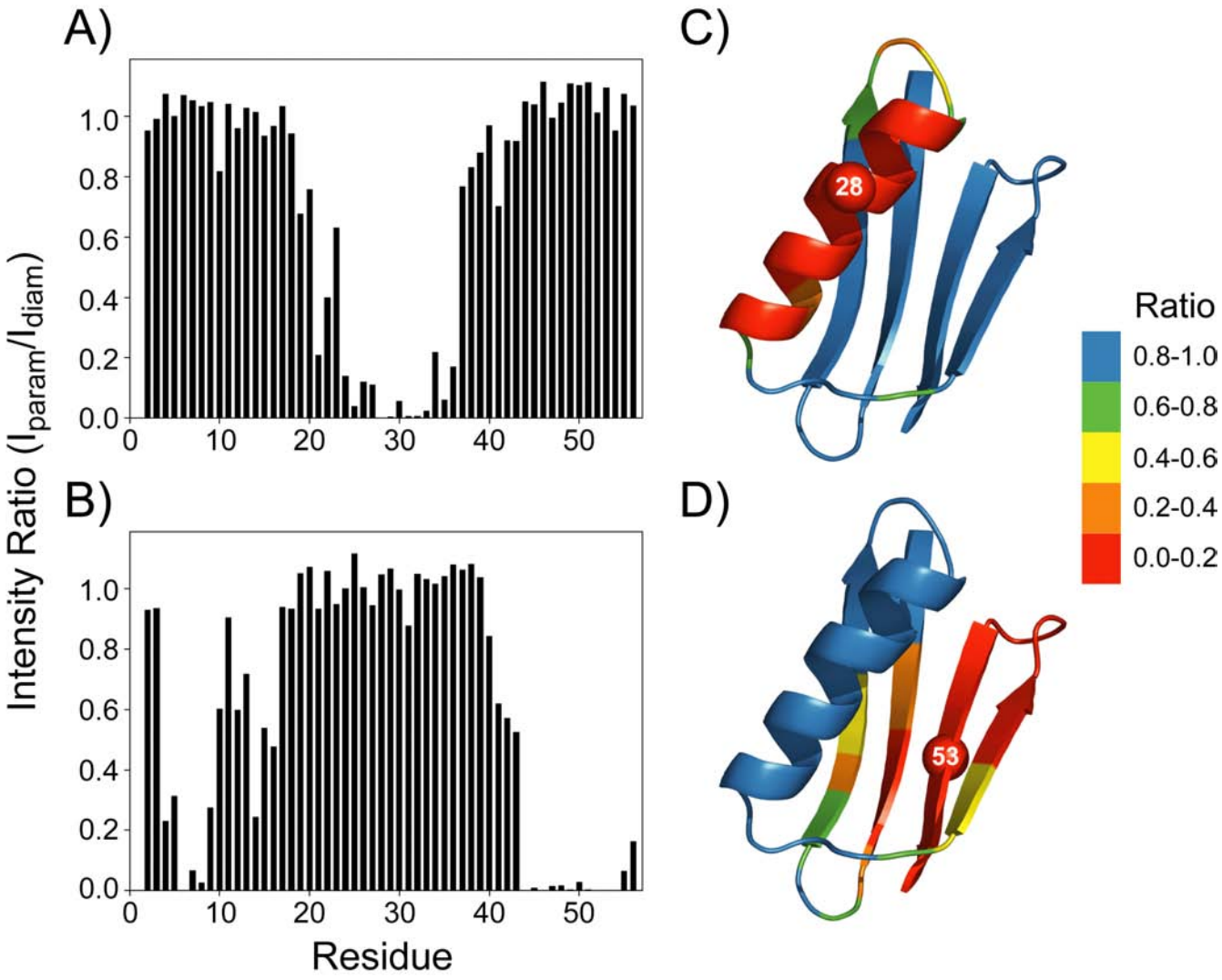

Figure S4. Summary of solution-state paramagnetic relaxation enhancements of amide ^{1}H and ^{15}N nuclei for 28R1 and 53R1. Ratios of peak intensities (heights) in ^{1}H-^{15}N HSQC spectra for spin labeled proteins relative to the corresponding ascorbate-reduced diamagnetic analogues are shown for 28R1 (A) and 53R1 (B), and mapped onto the ribbon diagram of wt GB1 (PDB ID: 1pga)[26] with the R1 modification sites indicated by spheres on the C^{α} atoms (C-D). For 28R1 the nuclei experiencing the largest PRE are found in the α-helix, while for 53R1 residues in the β1, β3, and β4 strands and the intervening loops (and to a lesser extent the β2-strand) are most strongly affected. The observed PREs are consistent with 28R1 and 53R1 both adopting a similar global fold to GB1 (as indicated by the chemical shift data in Figures S2 and S3).

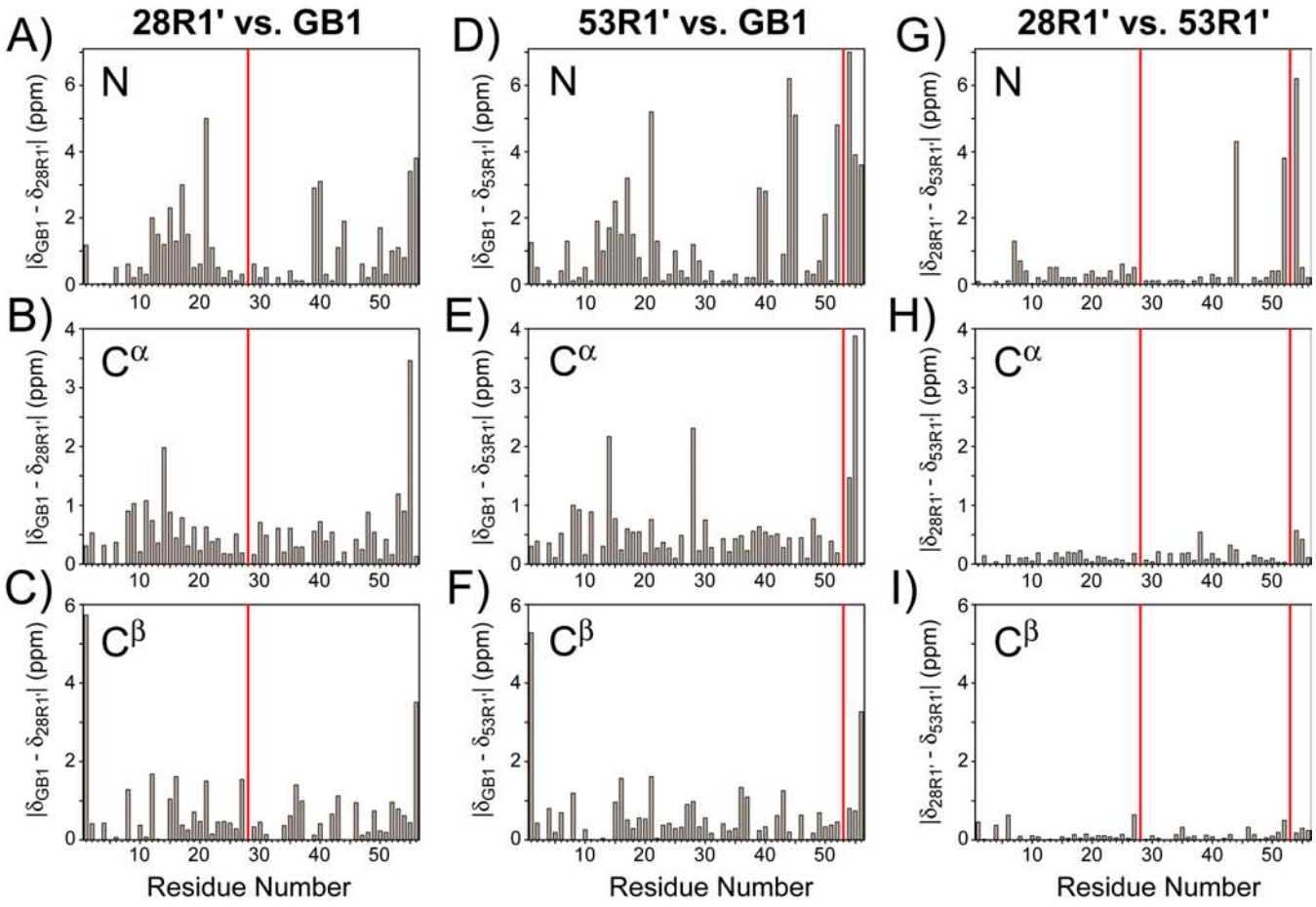

Figure S5. Quantitative analysis of solid-state NMR chemical differences for 28R1′ vs. wt GB1 (A-C), 53R1′ vs. wt GB1 (D-F) and 28R1′ vs. 53R1′ (G-I). 28R1′ and 53R1′ chemical shifts were obtained using 2D ^{13}C-^{13}C, ^{15}N-($^{13}C^{\alpha}$)-^{13}CX, and ^{15}N-($^{13}C'$)-^{13}CX experiments described above, and the published shifts[28] were used for GB1. Absolute chemical shift differences in ppm as a function of residue number are shown for ^{15}N, $^{13}C^{\alpha}$ and $^{13}C^{\beta}$ nuclei (nucleus type indicated directly in the plot), and the mutation sites (residues 28 and 53) are indicated by vertical red lines as applicable. For those residues where one or both shifts could not be determined the difference was set to zero in the plot and excluded from the calculated average. The average absolute chemical shift differences, $\langle|\Delta\delta|\rangle$, were (A-C) 28R1′ vs. GB1: $\langle|\Delta\delta(N)|\rangle = 1.0 \pm 1.1$ ppm, $\langle|\Delta\delta(C^{\alpha})|\rangle = 0.6 \pm 0.5$ ppm, $\langle|\Delta\delta(C^{\beta})|\rangle = 0.8 \pm 1.0$ ppm; (D-F) 53R1′ vs. GB1: $\langle|\Delta\delta(N)|\rangle = 1.5 \pm 1.8$ ppm, $\langle|\Delta\delta(C^{\alpha})|\rangle = 0.6 \pm 0.7$ ppm, $\langle|\Delta\delta(C^{\beta})|\rangle = 0.7 \pm 0.9$ ppm; (G-I) 28R1′ vs. 53R1′: $\langle|\Delta\delta(N)|\rangle = 0.6 \pm 1.2$ ppm, $\langle|\Delta\delta(C^{\alpha})|\rangle = 0.14 \pm 0.12$ ppm, $\langle|\Delta\delta(C^{\beta})|\rangle = 0.16 \pm 0.16$ ppm. In combination with the solution-state NMR results (Figures S2-S4), these data strongly suggest that 28R1 and 53R1 retain the GB1 fold in the microcrystalline state. Although the observed chemical shift differences for 28R1′ and 53R1′ (A-F) relative to published SSNMR shifts for GB1[28] are slightly larger that those observed in solution (Figure S3) the vast majority of the $^{13}C^{\alpha}$ and $^{13}C^{\beta}$ shifts are in reasonable agreement with the published values (within ~0.5 ppm). It is possible that these differences are at least in part due to slightly different NMR sample preparation conditions, experimental setup or slight differences in chemical shift referencing. Indeed, the comparison of 28R1′ and 53R1′ chemical shifts (G-I) indicates that for these samples, where identical conditions were used for sample preparation, data acquisition and analysis, the chemical shift differences are significantly reduced with the majority of the $^{13}C^{\alpha}$ and $^{13}C^{\beta}$ deviations within ~0.1 ppm.

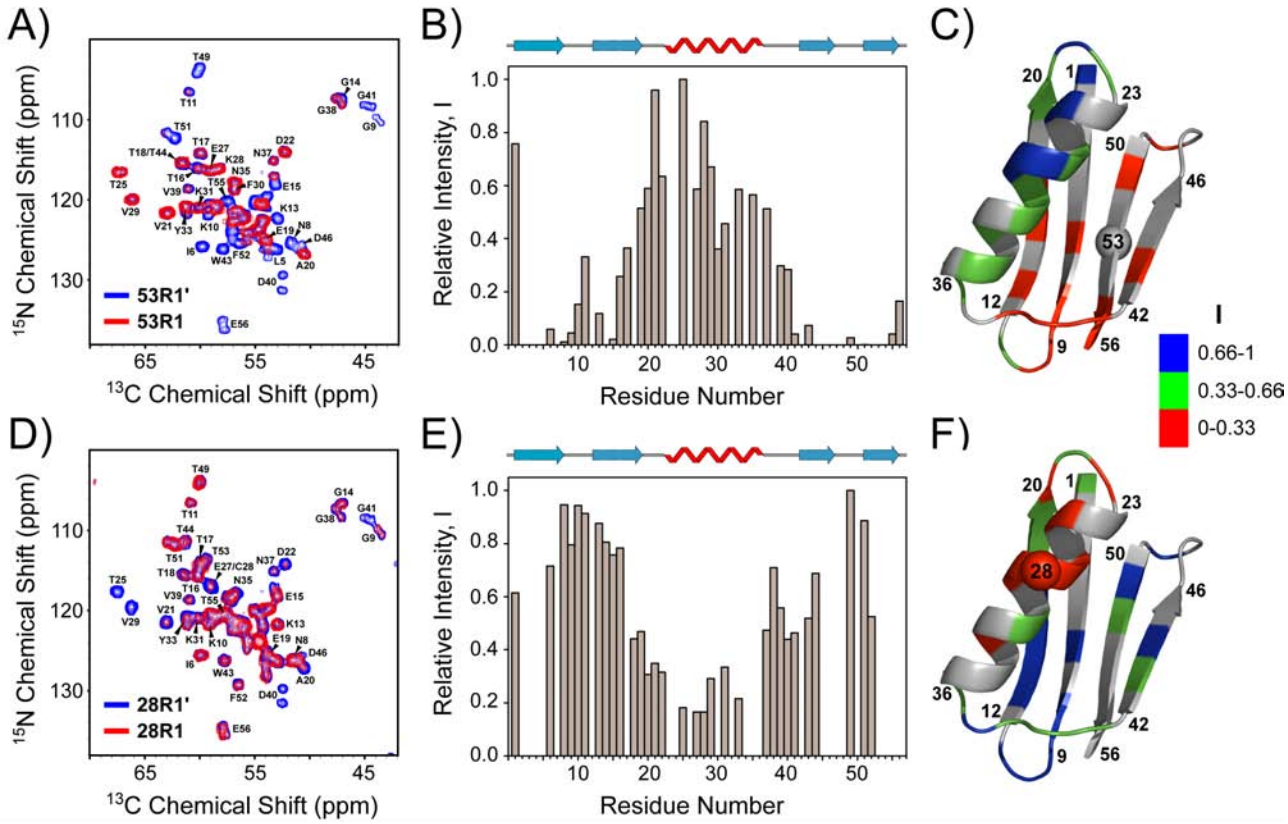

Figure S6. (A,D) 500 MHz 2D ^{15}N-^{13}C$^{\alpha}$ correlation spectra of (A) microcrystalline 53R1 (red) and 53R1′ (blue), and (D) 28R1 (red) and 28R1′ (blue), acquired at 11.111 kHz MAS. Relatively short magnetization transfer steps were used (0.15 and 3 ms for ^{1}H-^{15}N and ^{15}N-^{13}C$^{\alpha}$ CP, respectively) to minimize the transverse magnetization decay for the R1 samples as discussed in the text (c.f., Figures S8-S10). Typical acquisition parameters used for 53R1′ (~4 mg of protein) were as follows: 48* (t_1, ^{15}N) × 1500* (t_2,^{13}C) data matrix with time increments of (360, 20) μs resulting in acquisition times of (16.9, 30.0) ms, 2.5 s recycle delay, 256 transients per FID, total measurement time ~17 h. Data sets were processed in NMRPipe[13] by using 63^{o}-shifted sine and sine-squared window functions in the ^{15}N and ^{13}C dimensions, respectively, and zero-filled to 512 (^{15}N) and 4096 (^{13}C) points. This resulted in ^{15}N-^{13}C$^{\alpha}$ correlations with an average S/N ratio of ~50:1. Resonance assignments (obtained using 2D ^{13}C-^{13}C, ^{15}N-(^{13}C$^{\alpha}$)-^{13}CX, and ^{15}N-(^{13}C′)-^{13}CX experiments and summarized in Figure S5) corresponding to relatively well-resolved ^{15}N-^{13}C$^{\alpha}$ cross-peaks are indicated in the spectra. We note here that several residues in 28R1/28R1′ and 53R1/53R1′, especially those found in or near the loops and termini (e.g., G9, G38, V39, D40, G41, T49, E56), appear to give rise to correlations displaying increased inhomogeneous broadening or peak doubling (particularly in the ^{15}N dimension), and these spectral features were reproducibly observed in several microcrystalline 28R1/28R1′ and 53R1/53R1′ samples prepared at different times. Although their exact origin is not fully understood yet, these features are likely caused by increased conformational heterogeneity (static disorder) in the loop regions of 28R1/28R1′ and 53R1/53R1′ in the microcrystalline state, and attempts to prepare more homogeneous protein microcrystals are ongoing. Interestingly, microcrystalline samples of wt GB1 or the closely-related B3 immunoglobulin-binding domain of protein G (GB3) prepared in our laboratory under analogous conditions did not exhibit these types of spectral features (data not shown). (B,E) Relative cross-peak intensities (heights), I, in (B) 53R1/53R1′ and (E) 28R1/28R1′ as a function of residue number. To account for possible differences in the amount of ^{13}C,^{15}N-protein in R1 and R1′ samples, we define $I = (I_{R1}/I_{R1'})/(I_{R1}/I_{R1'})_{max}$, where I_{R1} and $I_{R1'}$ are the peak heights in R1 and R1′ spectra and $(I_{R1}/I_{R1'})_{max}$ is the maximum $(I_{R1}/I_{R1'})$ value for the R1/R1′ pair (found here to be ~0.7-0.8). Peak heights were extracted using Sparky[14] (for peaks with severely reduced intensity in the R1 spectrum, the intensity at the exact peak position in the R1′ spectrum was used) and for peaks where no quantitative measurement could be made due to overlap, I was set to zero. (C,F) Ribbon diagram of GB1 (PDB ID: 1pga), with the I values determined for (C) 53R1/53R1′ and (F) 28R1/28R1′ mapped onto the structure and color coded as indicated in the figure. Residues for which I was not determined are colored in gray, and the R1/R1′ incorporation sites (residues 28 and 53) are indicated by spheres on the C$^{\alpha}$ atom.

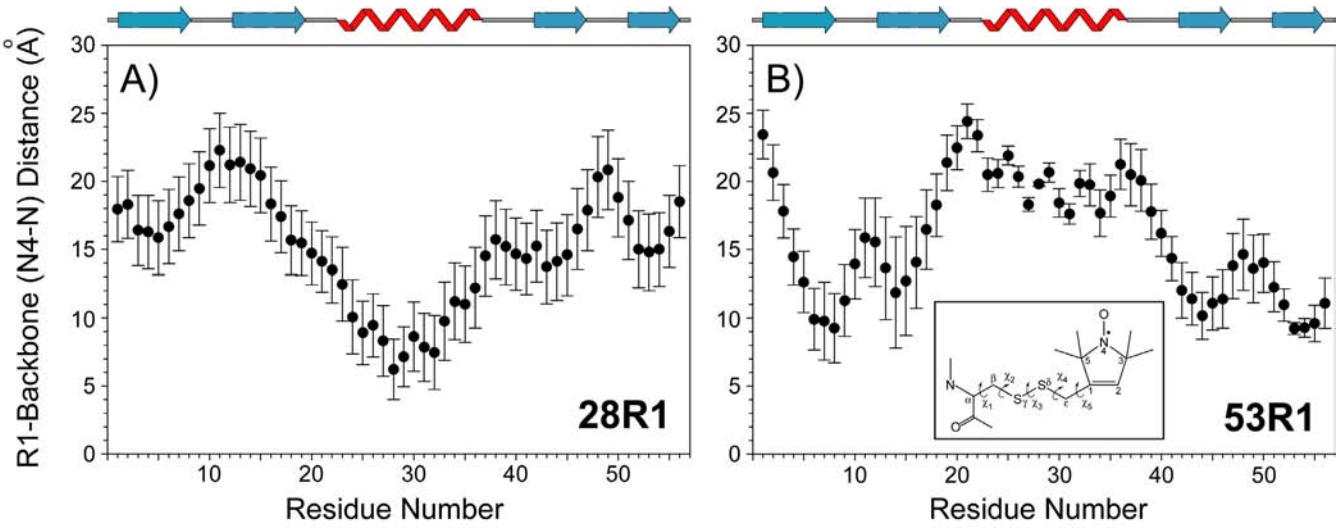

Figure S7. Estimated distances between the R1 nitrogen atom (N4) and protein backbone amide nitrogens as a function of residue number for 28R1 (A) and 53R1 (B). The structure of the R1 side-chain, indicating dihedral angles χ_1-χ_5 (defined as $\chi_1 \equiv$ N-Cα-Cβ-Sγ, $\chi_2 \equiv$ Cα-Cβ-Sγ-Sδ, $\chi_3 \equiv$ Cβ-Sγ-Sδ-Cε, $\chi_4 \equiv$ Sγ-Sδ-Cε-C1, $\chi_5 \equiv$ Sδ-Cε-C1-C2) is shown in the inset of (B). In order to estimate the distances we started from atomic coordinate (PDB) files of wt GB1 (PDB ID: 1pga), containing R1 in positions 28 or 53 (created using the XLEaP module of the program AMBER[29]), and generated several GB1 structural models with different R1 side-chain conformations using the program PyMOL.[30] Although R1 has five rotatable bonds and therefore, in principle at least, a large number of possible conformations, only a relatively small number of these need to be considered to obtain an approximate separation between the spin label and the protein backbone atoms. First, as discussed by Hubbell and co-workers,[31] the preferred configurations of R1 at α-helix surface sites not involved in significant crystal contacts are g^+g^+ (i.e., $\chi_1 = \chi_2 = -60^o$) and, to a lesser extent, tg^- (i.e., $\chi_1 = 180^o$, $\chi_2 = +60^o$) (note that these χ_1 values also account for over 85% of cysteine side-chain conformations in a rotamer library of 132 proteins[32]). Second, rotation about the Cε-C1 bond (i.e., χ_5) has a negligible effect on the R1-backbone distances (typically < 1 Å) relative to χ_3 and χ_4 rotations. With these considerations we have generated for 28R1 (corresponding to a relatively unobstructed α-helix surface site) an ensemble of 18 structures with R1 in the g^+g^+ or tg^- χ_1, χ_2 configuration, $\chi_5 = 90^o$ and all possible combinations of -60^o (g^+), $+60^o$ (g^-) and 180^o (t) for χ_3 and χ_4. Although a few χ_1-χ_5 configurations (e.g., $g^+g^+g^-g^-90$) did exhibit apparent steric clashes with the protein backbone most structures were free of these, and, for completeness, all 18 structures in the ensemble were considered in the estimation of the average distances reported in (A). For each residue the distances to the R1 N4 atom observed for the ensemble were relatively uniformly distributed within the observed ranges with deviations of ca. ±2.5 Å from the average distance. For 53R1, which corresponds to a relatively restricted solvent-exposed R1 site in a β-sheet, the majority of R1 conformations investigated exhibited severe steric clashes with the protein backbone and/or sidechains. Therefore, in this case we have selected three representative R1 conformers (χ_1-χ_5 = {-160,180,160,90,20}, {60,180,-120,180,20}, {60,180,60,180,20}), which were free of obvious clashes with the protein atoms and corresponded to approximately the largest changes in the spin label position. The average distances between the protein backbone amide nitrogens and R1 N4 in these conformers are shown in (B) and also exhibit deviations of ca. ±2-2.5 Å on average. Remarkably, for both 28R1 and 53R1 the protein backbone-spin label distances estimated using this rather simplistic approach, are in reasonable agreement with the cross-peak intensity patterns observed in the 2D ^{15}N-^{13}C$^{\alpha}$ correlation spectra (c.f., Figure 1 and S6).

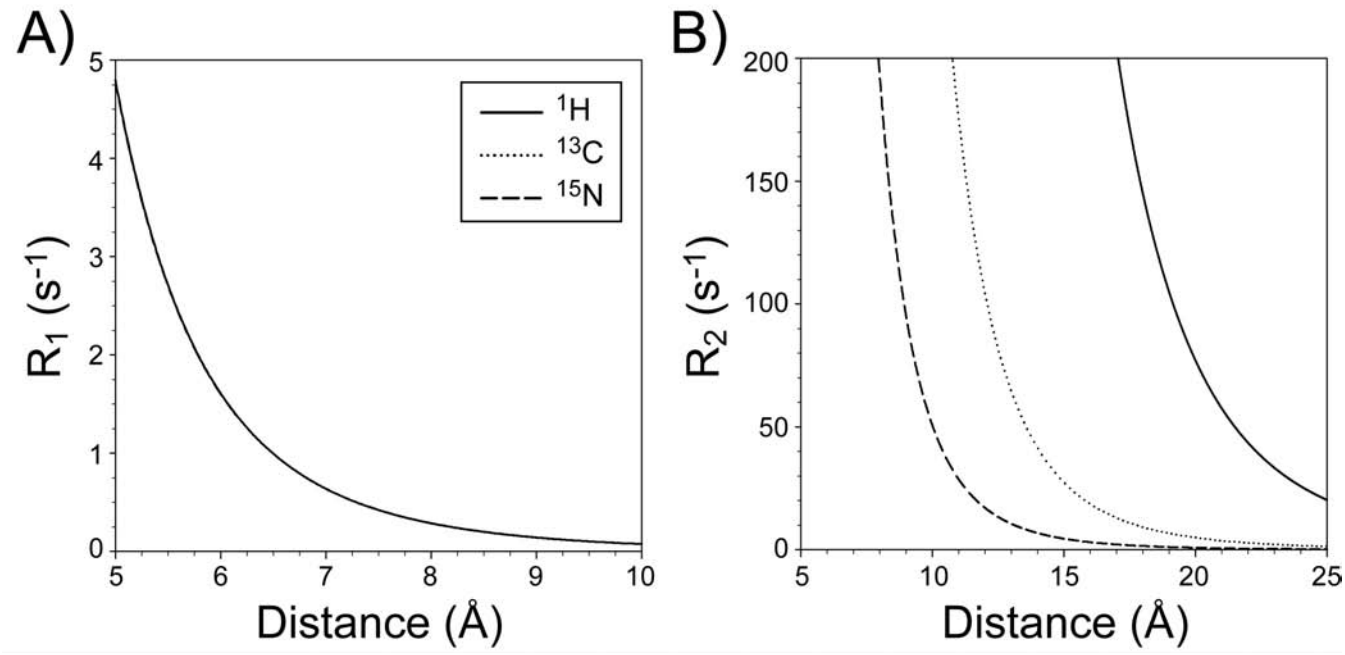

Figure S8. Dipolar contribution to (A) longitudinal, R_1, and (B) transverse, R_2, nuclear spin relaxation due to the presence of an unpaired electron in the solid-state (i.e., only electron spin relaxation contributes to the overall correlation time, τ_c), calculated as a function of the electron-nucleus distance using the Solomon-Bloembergen equations.[33,34] The calculations were performed for a ^{1}H, ^{13}C, or ^{15}N nucleus (see figure legend) and a nitroxide spin label (S = ½) at B_0 = 11.7 T, assuming g = 2.0023 and $\tau_c = T_{1e} = T_{2e}$ = 100 ns.[34-36]

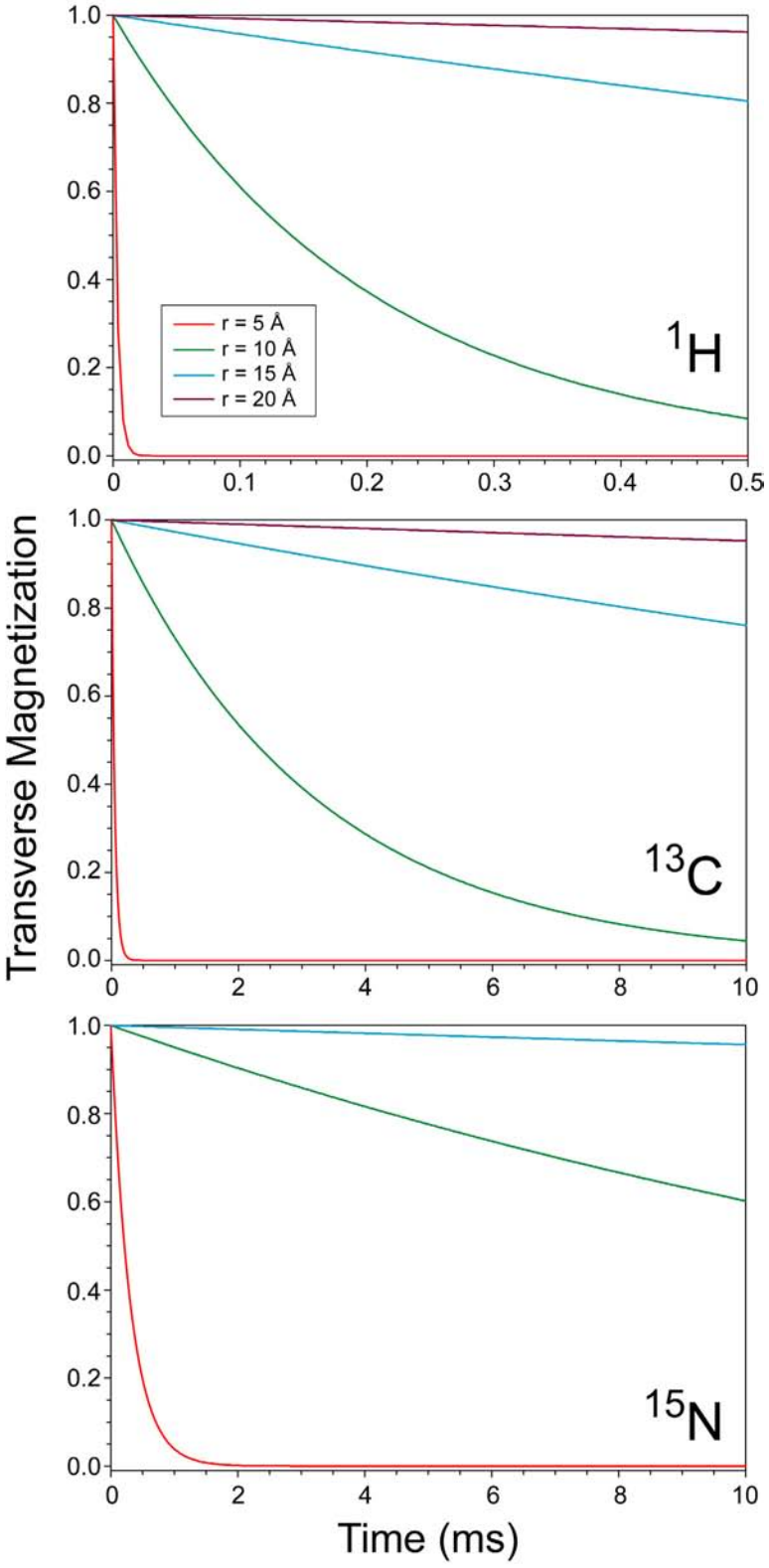

Figure S9. Calculated decay of transverse magnetization as a function of time, $M_{x,y} = \exp(-R_2 t)$, for ^{1}H (top), ^{13}C (middle) and ^{15}N (bottom) nuclei at distances of 5 Å (red), 10 Å (green), 15 Å (blue) and 20 Å (magenta) from a nitroxide radical. The R_2 values for each distance and nucleus combination were calculated using the Solomon-Bloembergen equations with the parameters given in the Figure S8 caption. Since under typical experimental conditions $R_{1\rho} \approx R_2$,[34,37] the same decay profiles are expected to apply to transverse magnetization during a spin-lock pulse (c.f., Figure S10).

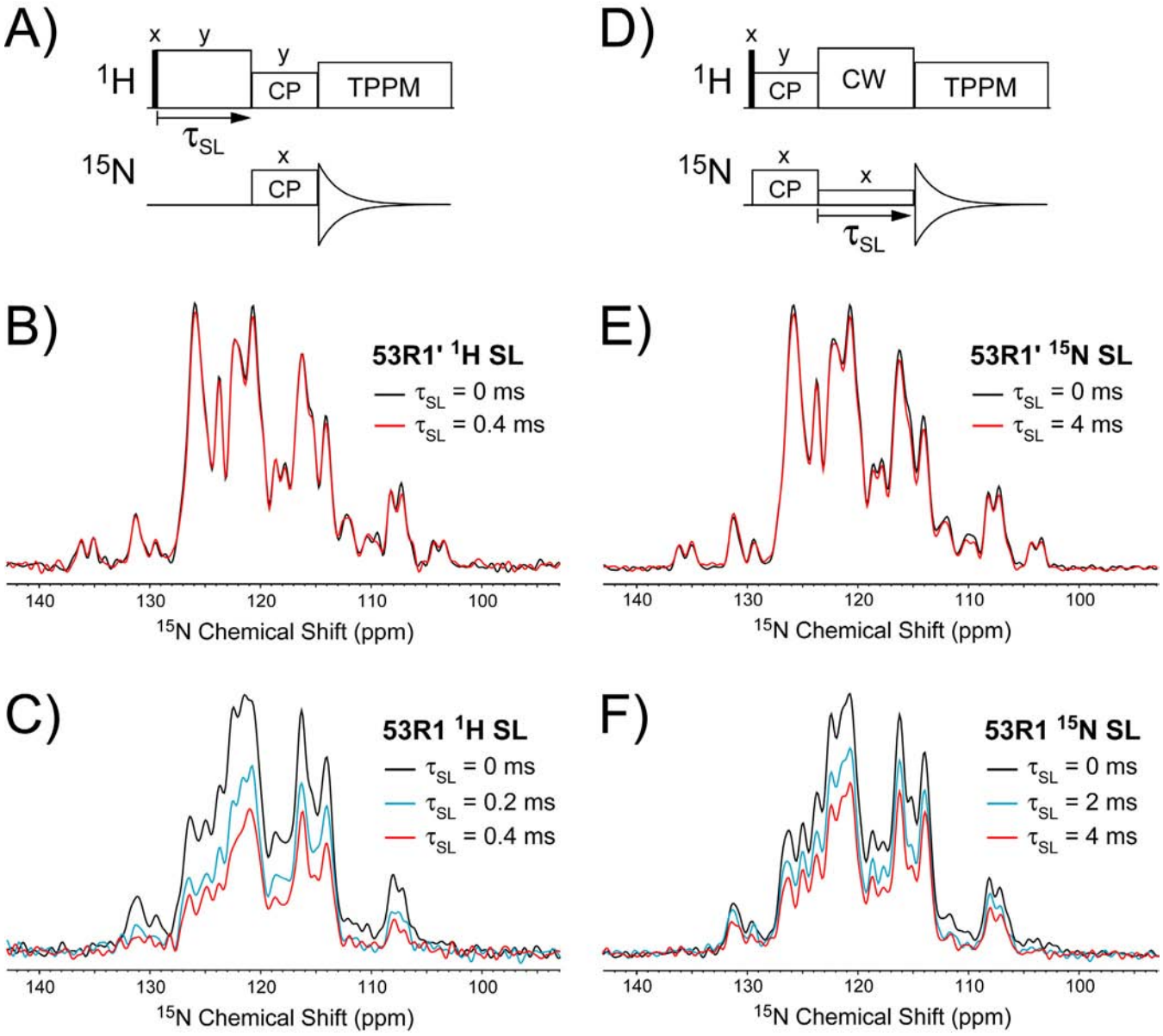

Figure S10. Measurement of transverse ^{1}H (A-C) and ^{15}N (D-F) magnetization decay during a spin-lock (SL) pulse (i.e., $R_{1\rho}$) for 53R1 and 53R1′. (A) Pulse scheme used for ^{15}N-detected ^{1}H $R_{1\rho}$ measurement: 90° — ^{1}H SL — ^{1}H-^{15}N CP — acquire. SL: ^{1}H field ~100 kHz; ^{1}H-^{15}N CP: ^{1}H field ~50 kHz, ^{15}N field ~40 kHz, 150 μs contact time; TPPM decoupling: ^{1}H field ~70 kHz, pulse length 7.0 μs, total phase difference 7.0°. (B) ^{15}N spectra of 53R1′ recorded with ^{1}H SL pulses of duration τ_{SL} = 0 (black) and τ_{SL} = 0.4 ms (red). (C) ^{15}N spectra of 53R1 recorded with ^{1}H SL pulses of duration τ_{SL} = 0 (black), τ_{SL} = 0.2 ms (cyan), and τ_{SL} = 0.4 ms (red). (D) Pulse scheme used for ^{15}N $R_{1\rho}$ measurement: 90° — ^{1}H-^{15}N CP — ^{15}N SL — acquire. SL: ^{15}N field ~27 kHz, ^{1}H decoupling field ~100 kHz. ^{1}H-^{15}N CP and TPPM parameters same as in (A). (E) ^{15}N spectra of 53R1′ recorded with ^{15}N SL pulses of duration τ_{SL} = 0 (black) and τ_{SL} = 4 ms (red). (F) ^{15}N spectra of 53R1 recorded with ^{15}N SL pulses of duration τ_{SL} = 0 (black), τ_{SL} = 2 ms (cyan), and τ_{SL} = 4 ms (red). Similar results were obtained for 28R1 and 28R1′ (data not shown).

References

(1) Smith, C. K.; Withka, J. M.; Regan, L. *Biochemistry* **1994,** 33, 5510-5517.
(2) Rost, B.; Sander, C. *Proteins* **1994,** 20, 216-226.
(3) Battiste, J. L.; Wagner, G. *Biochemistry* **2000,** 39, 5355-5365.
(4) Mchaourab, H. S.; Lietzow, M. A.; Hideg, K.; Hubbell, W. L. *Biochemistry* **1996,** 35, 7692-7704.
(5) Liang, B.; Bushweller, J. H.; Tamm, L. K. *J. Am. Chem. Soc.* **2006,** 128, 4389-4397.
(6) Cai, M. L.; Huang, Y.; Sakaguchi, K.; Clore, G. M.; Gronenborn, A. M.; Craigie, R. *J. Biomol. NMR* **1998,** 11, 97-102.
(7) Hubbell, W. L.; Altenbach, C. *Curr. Opin. Struct. Biol.* **1994,** 4, 566-573.
(8) Berliner, L. J.; Grunwald, J.; Hankovszky, H. O.; Hideg, K. *Anal. Biochem.* **1982,** 119, 450-455.
(9) Kocherginsky, N.; Swartz, H. M., *Nitroxide spin labels. Reactions in biology and chemistry*. CRC Press: Boca Raton, FL, 1995.
(10) Onishi, H.; Morales, M. F. *Arch. Biochem. Biophys.* **1976,** 172, 12-19.
(11) Gross, A.; Columbus, L.; Hideg, K.; Altenbach, C.; Hubbell, W. L. *Biochemistry* **1999,** 38, 10324-10335.
(12) Yamazaki, T.; Lee, W.; Arrowsmith, C. H.; Muhandiram, D. R.; Kay, L. E. *J. Am. Chem. Soc.* **1994,** 116, 11655-11666.
(13) Delaglio, F.; Grzesiek, S.; Vuister, G. W.; Zhu, G.; Pfeifer, J.; Bax, A. *J. Biomol. NMR* **1995,** 6, 277-293.
(14) Goddard, T. D.; Kneller, D. G., University of California, San Francisco.
(15) Stringer, J. A.; Bronnimann, C. E.; Mullen, C. G.; Zhou, D. H. H.; Stellfox, S. A.; Li, Y.; Williams, E. H.; Rienstra, C. M. *J. Magn. Reson.* **2005,** 173, 40-48.
(16) Bielecki, A.; Burum, D. P. *J. Magn. Reson. A* **1995,** 116, 215-220.
(17) Bennett, A. E.; Rienstra, C. M.; Auger, M.; Lakshmi, K. V.; Griffin, R. G. *J. Chem. Phys.* **1995,** 103, 6951-6957.
(18) Baldus, M.; Petkova, A. T.; Herzfeld, J.; Griffin, R. G. *Mol. Phys.* **1998,** 95, 1197-1207.
(19) Hediger, S.; Meier, B. H.; Ernst, R. R. *Chem. Phys. Lett.* **1995,** 240, 449-456.
(20) Pauli, J.; Baldus, M.; van Rossum, B.; de Groot, H.; Oschkinat, H. *ChemBiochem* **2001,** 2, 272-281.
(21) Metz, G.; Wu, X.; Smith, S. O. *J. Magn. Reson. A* **1994,** 110, 219-227.
(22) Zilm, K. W. In 40th Experimental NMR Conference, Orlando, FL, 1999.
(23) Takegoshi, K.; Nakamura, S.; Terao, T. *Chem. Phys. Lett.* **2001,** 344, 631-637.
(24) Marcombe, C. R.; Gaponenko, V.; Byrd, R. A.; Zilm, K. W. *J. Am. Chem. Soc.* **2004,** 2004, 7196-7197.
(25) Marcombe, C. R.; Zilm, K. W. *J. Magn. Reson.* **2003,** 162, 479-486.
(26) Gallagher, T.; Alexander, P.; Bryan, P.; Gilliland, G. L. *Biochemistry* **1994,** 33, 4721-4729.
(27) Gronenborn, A. M.; Clore, G. M. *J. Mol. Biol.* **1993,** 233, 331-335.
(28) Franks, W. T.; Zhou, D. H.; Wylie, B. J.; Money, B. G.; Graesser, D. T.; Frericks, H. L.; Sahota, G.; Rienstra, C. M. *J. Am. Chem. Soc.* **2005,** 127, 12291-12305.
(29) Pearlman, D. A.; Case, D. A.; Caldwell, J. W.; Ross, W. S.; Cheatham III, T. E.; DeBolt, S.; Ferguson, D.; Seibel, G.; Kollman, P. *Comp. Phys. Commun.* **1995,** 91, 1-41.
(30) DeLano, W. L., The PyMOL Molecular Graphics System (2002) DeLano Scientific, Palo Alto, CA, USA. http://www.pymol.org.
(31) Langen, R.; Oh, K. J.; Cascio, D.; Hubbell, W. L. *Biochemistry* **2000,** 39, 8396-8405.
(32) Dunbrack, R. L.; Karplus, M. *J. Mol. Biol.* **1993,** 230, 543-574.
(33) Solomon, I. *Phys. Rev.* **1955,** 99, 559-565.
(34) Bertini, I.; Luchinat, C. *Coord. Chem. Rev.* **1996,** 150, 1-292.
(35) Kosen, P. A. *Meth. Enzymol.* **1989,** 177, 86-121.
(36) Eaton, S. S.; Eaton, G. R., In *Biological Magnetic Resonance, Volume 19: Distance Measurements in Biological Systems by EPR*, Kluwer Academic: New York, 2000.
(37) Koenig, S. H. *J. Magn. Reson.* **1982,** 47, 441-453.